Conformational switching of the 26S proteasome enables substrate degradation
Mary E. Matyskiela, Gabriel C. Lander & Andreas Martin
Supplementary Figures

Supplementary Figure 1

a

WT particles in the absence of substrate (side view class averages and variance)

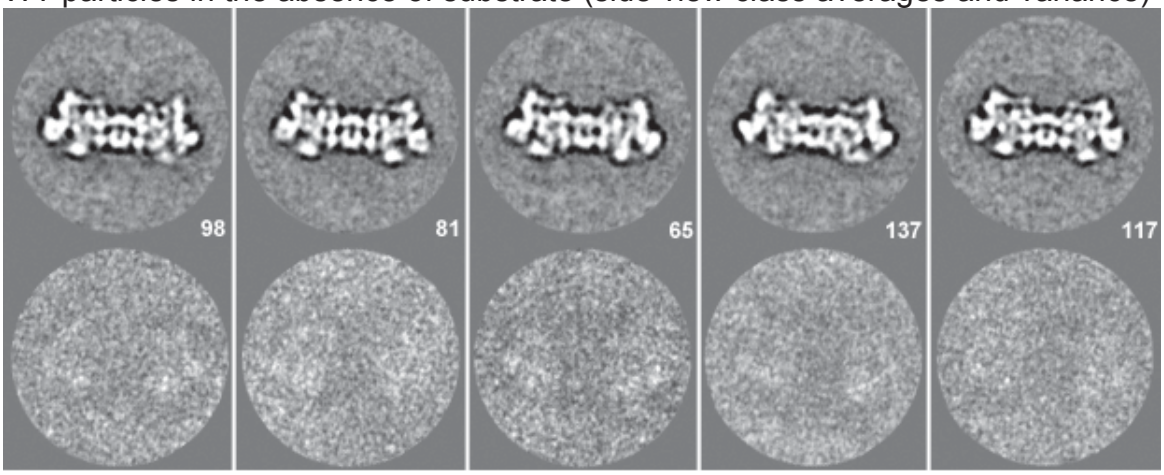

WT particles in the presence of substrate (side view class averages and variance)

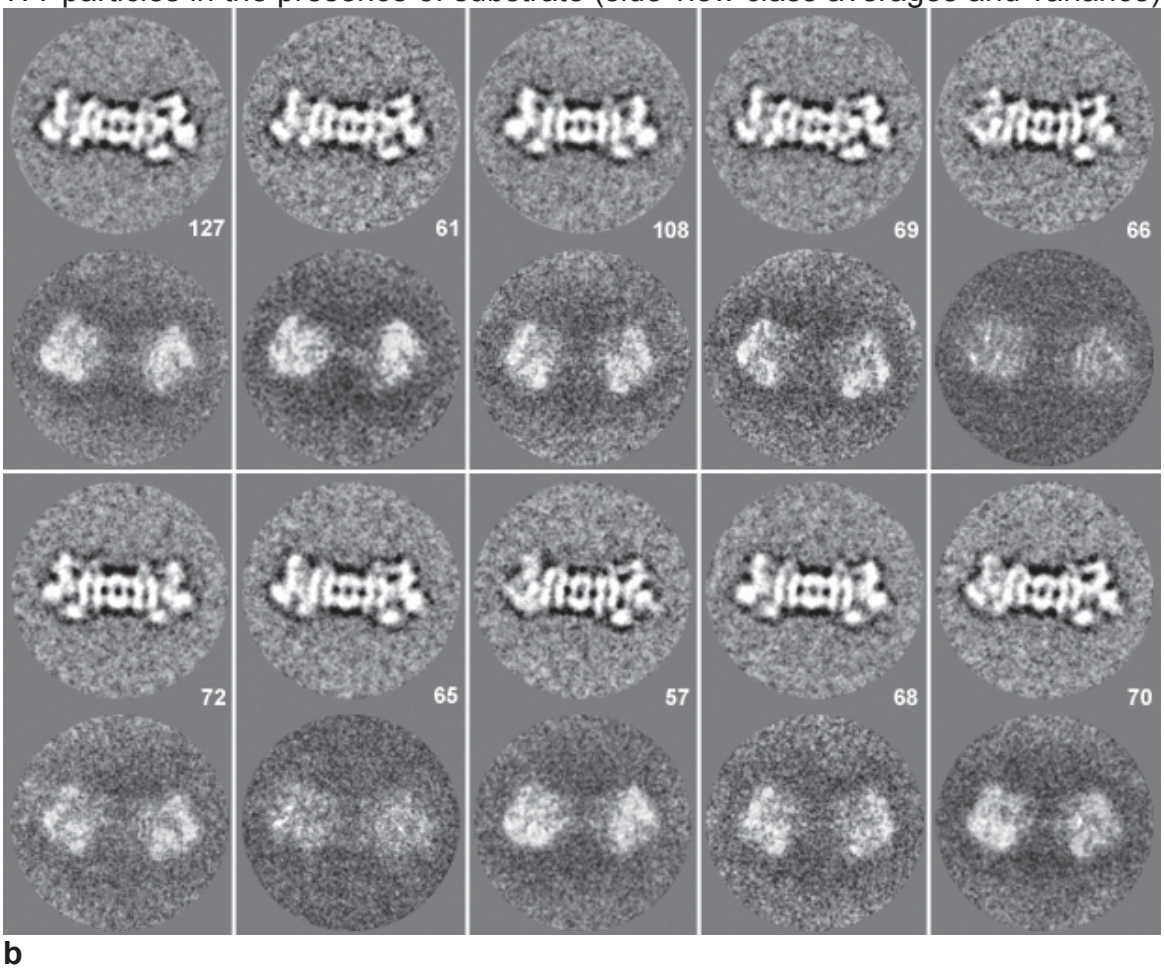

b

Rpn11^{AXA} Rpn13Δ mutant particles in the absence of substrate (side view class averages and variance)

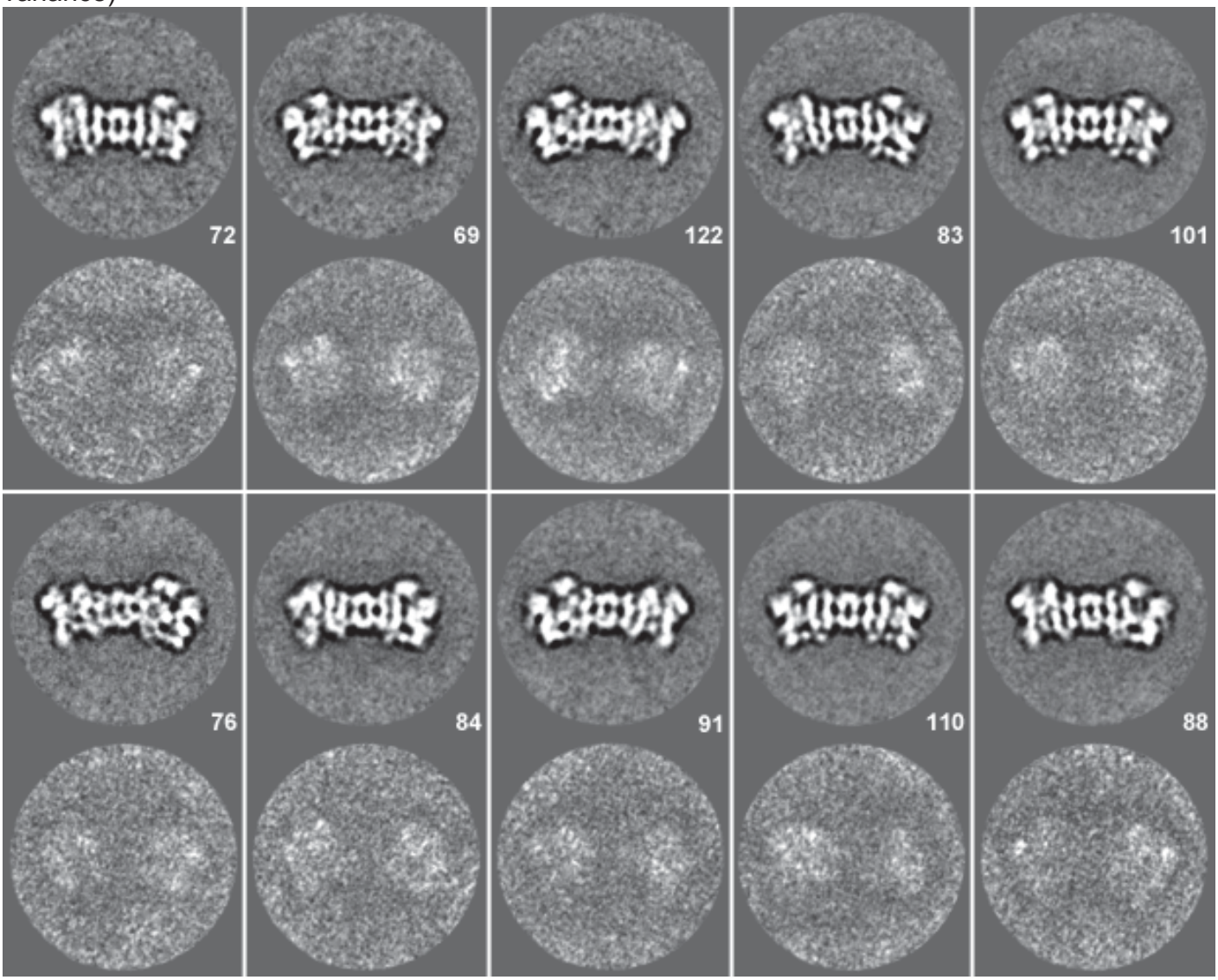

c

Rpn11^{AXA} Rpn13Δ mutant particles in the presence of substrate (side view class averages and variance)

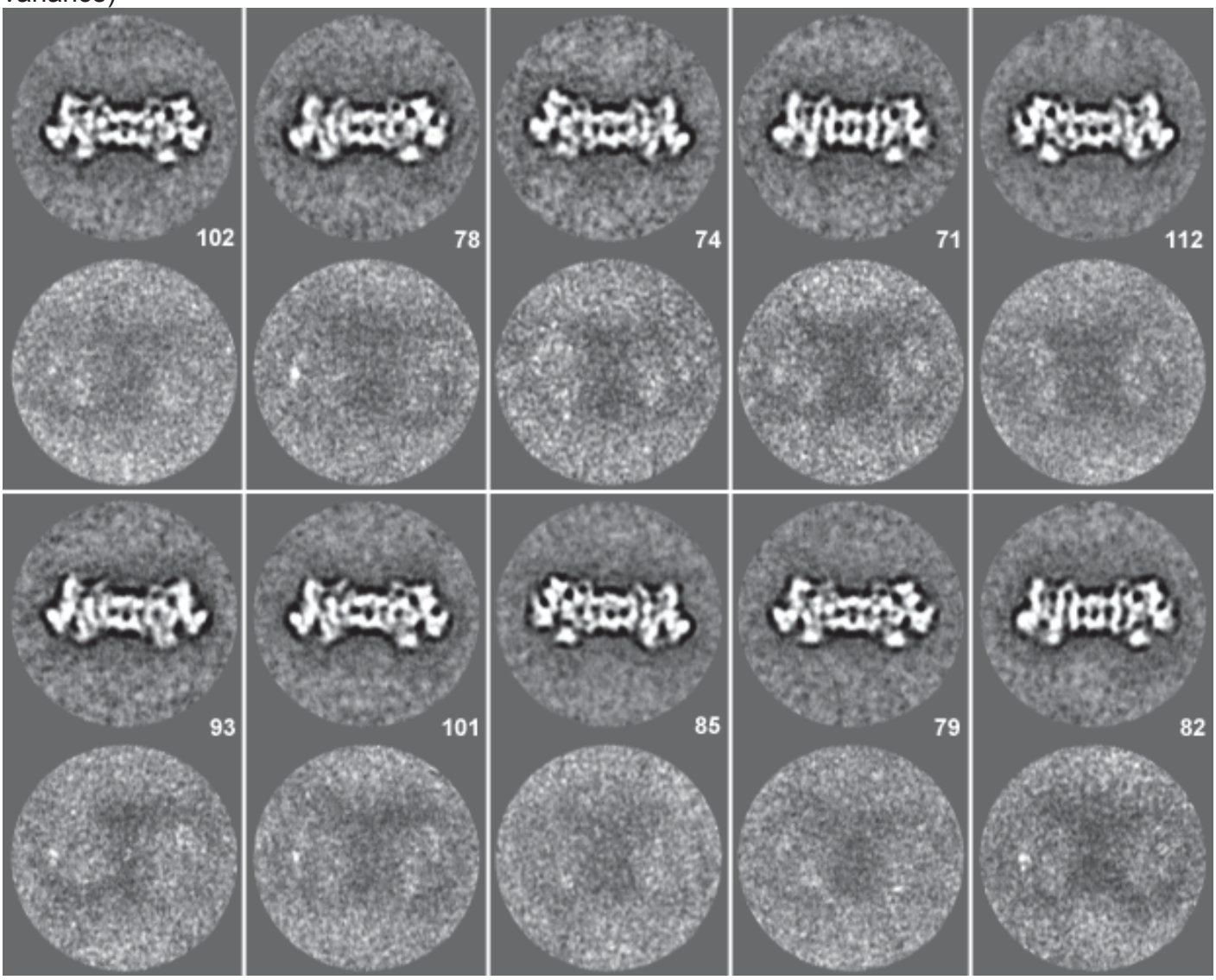

d

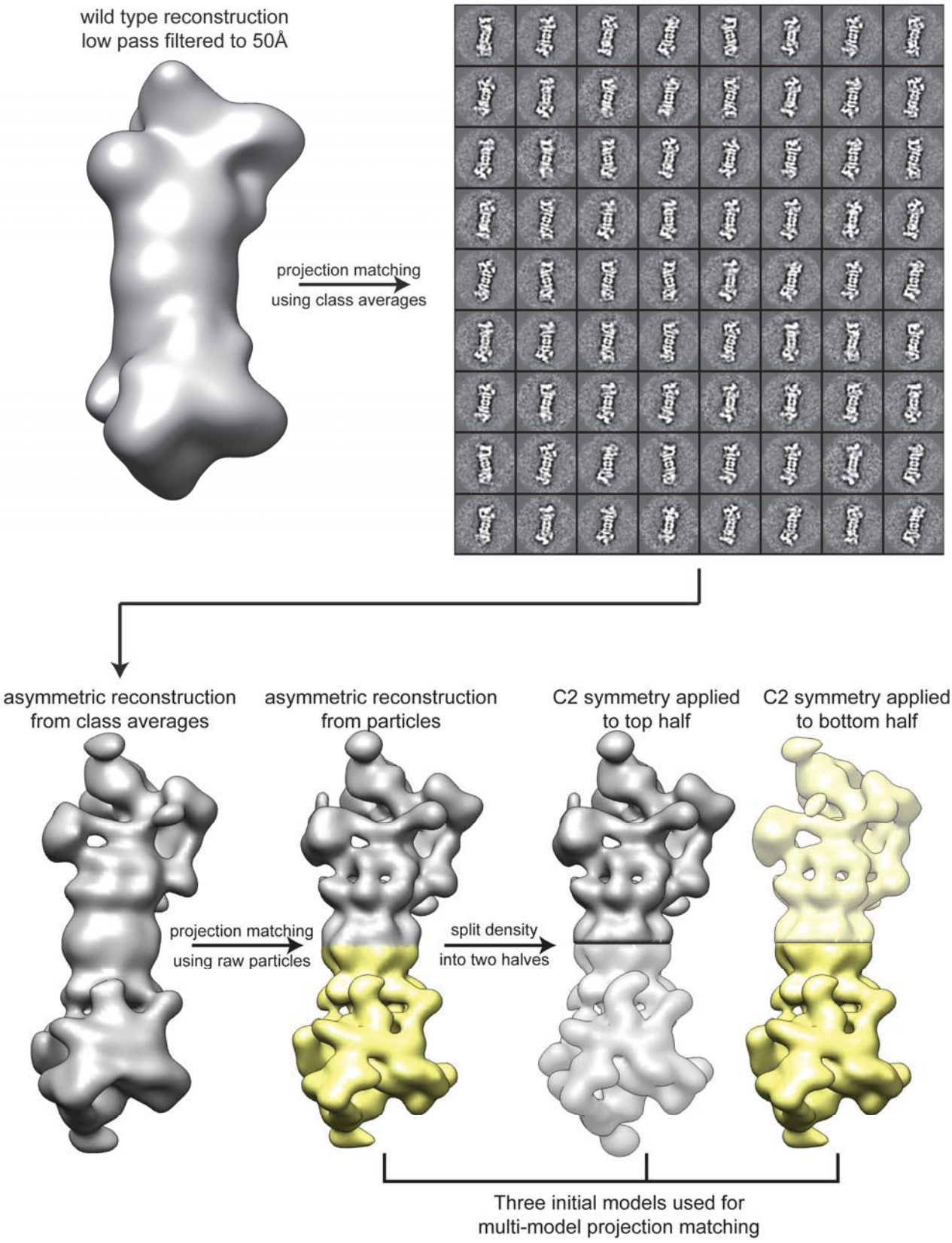
wild type reconstruction
low pass filtered to 50Å
projection matching
using class averages
asymmetric reconstruction
from class averages
asymmetric reconstruction
from particles
C2 symmetry applied
to top half
C2 symmetry applied
to bottom half
projection matching
using raw particles
split density
into two halves
Three initial models used for
multi-model projection matching

e

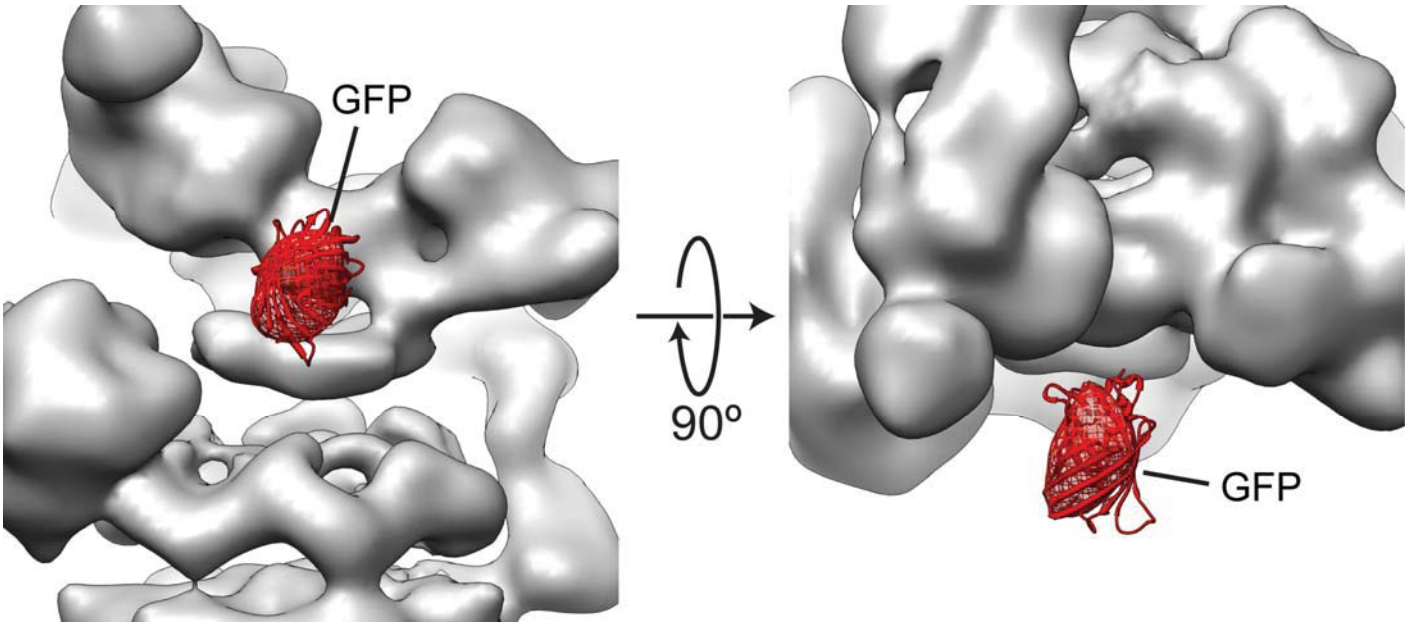

Supplementary Figure 1. 2D and 3D analyses of proteasome particles in the absence and presence of substrate. (**a**) Wild-type (WT) particles in the presence of substrate exhibit high levels of variance at the regulatory particles, indicating a high degree of conformational heterogeneity in this region. The number of particles contributing to each class average is shown to the right of the average. (**b**) Although Rpn11^{AXA} Rpn13Δ mutant particles in the absence of substrate exhibit some variance at the regulatory particle, it is significantly less than the variability observed for wild type particles in the presence of substrate. (**c**) The regulatory particle of the Rpn11AXA Rpn13Δ mutant in the presence of substrate shows very little variance, indicating that the vast majority of these particles are trapped in a single conformation. Small points of variance at the periphery of the regulatory particles may correspond to ubiquitin or substrate associated with the proteasome. (**d**) 3D analysis of wild-type proteasome particles in the presence of substrate. The previously determined C2-symmetric wild type proteasome reconstruction (EMDB-1992) was low-pass filtered to 50 Å resolution, and used to assign 3D orientations to reference-free class averages of proteasome particles in the presence of substrate (see methods). Back-projection of these class averages provided a low-resolution asymmetric density, which was used as an initial model for projection matching with raw particles, resulting in a structure that contained 2 regulatory particles that were in distinct conformations. This reconstruction was split into two halves, and C2 symmetry was applied to each half to generate proteasome models that contained a single conformational state at both ends. These three models were used for subsequent multi-model projection matching with the raw particles. (**e**) Additional density in the reconstruction of wild-type particles in the presence of substrate. The density observed near the entrance to the ATPase ring when excess substrate is added to wild type particles accommodates a GFP molecule. The low resolution of the reconstruction and the inherent flexibility of the substrate result in a density that does not accurately encompass the molecular envelope of the docked GFP, but the overall size is indicative of a stalled molecule at this position.

Supplementary Figure 2

a

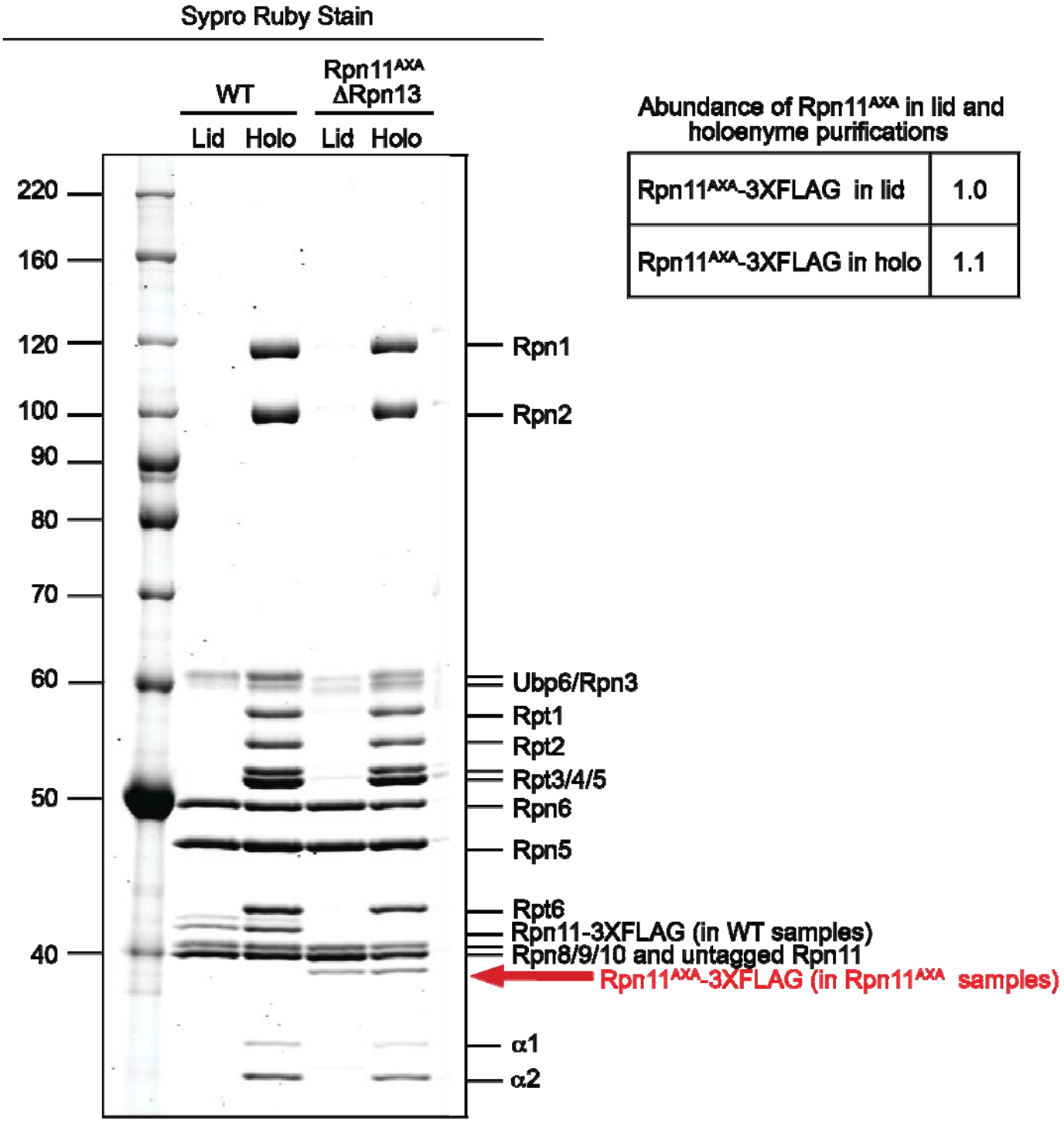

Abundance of $Rpn11^{AXA}$ in lid and holoenyme purifications

$Rpn11^{AXA}$-3XFLAG in lid	1.0
$Rpn11^{AXA}$-3XFLAG in holo	1.1

b

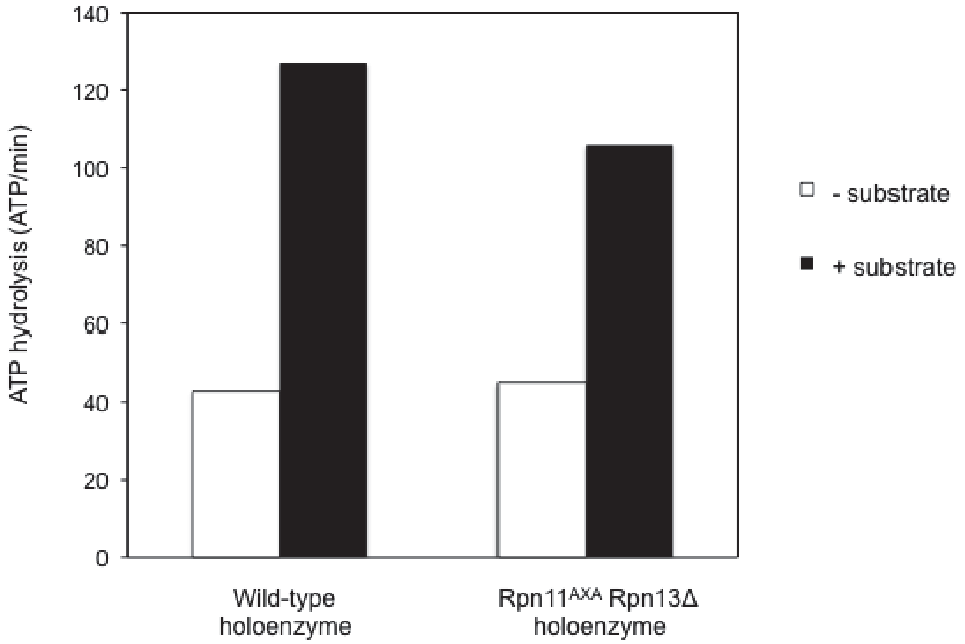

Supplementary Figure 2. Characterization of the composition and ATPase activity of the Rpn11^{AXA} Rpn13Δ holoenzyme.

(**a**) Abundance of Rpn11^{AXA} in purified mutant holoenzyme. Since the Rpn11^{AXA} mutation is lethal, Rpn11^{AXA} -3XFLAG proteasome was purified from a yeast strain that contained an additional untagged wild-type copy of Rpn11. Doubly-capped proteasome that was affinity-purified from this strain may thus contain wild-type (WT) Rpn11 in one of the two caps. To assess the relative amount of mutant Rpn11^{AXA} in the proteasome sample, we analyzed the band intensities of isolated lid and holoenzyme samples on a Sypro Ruby stained Tris-glycine SDS-PAGE gel (10%). Mutant Rpn11^{AXA}-3XFLAG (red arrow) runs significantly different from untagged wild-type Rpn11, which co-migrates with Rpn8 and Rpn9. For quantification, we calculated the abundance of Rpn11^{AXA}-FLAG relative to Rpn5 and Rpn6 for the isolated lid and holoenzyme samples. Since affinity-purified lid contains only a single, tagged copy of Rpn11, the amount of this Rpn11^{AXA}-3XFLAG was normalized to 1. The holoenzyme sample showed the same relative abundance of Rpn11^{AXA}-3XFLAG as the lid sample, indicating that this holoenzyme contained almost exclusively the mutant Rpn11^{AXA}. Proteasomes containing two FLAG-tagged copies of mutant Rpn11 apparently out-competed complexes with only a single tag during the affinity purification on limiting amounts of anti-FLAG M2 resin. (**b**) ATP-hydrolysis rate of wild-type and Rpn11^{AXA} Rpn13Δ proteasome is stimulated by substrate. ATP-hydrolysis by 300 nM wild-type (WT) or Rpn11^{AXA} Rpn13Δ holoenzyme was monitored by an NADH-coupled ATPase assay in the presence or absence of 10 μM ubiquitinated G3P substrate for 15 min. When wild-type proteasome is actively degrading ubiquitinated G3P substrate, its ATPase rate is stimulated 3-fold, from a basal rate of 43 ATP min^{-1} to 127 ATP min^{-1}. The ATPase rate of the Rpn11^{AXA} Rpn13Δ holoenzyme is also stimulated by substrate, from 45 ATP min^{-1} to 106 ATP min^{-1}, although this mutant is unable to degrade substrate at an appreciable rate. For the homologous unfoldase ClpX, substrates that pose a strong unfolding challenge do not stimulate the rate of ATP hydrolysis as much as substrates that are easily unfolded or readily translocated [2]. Correspondingly, when the ubiquitin chain on the G3P substrate cannot be removed by the Rpn11^{AXA} holoenzyme, the substrate becomes a more difficult unfolding challenge and the ATPase rate of the mutant enzyme is stimulated only 2.3-fold. Notably, even though the Rpn11^{AXA} Rpn13Δ holoenzyme stalls on the ubiquitinated substrate, this stalled state appears to be dynamic, with the enzyme continuing to hydrolyze ATP and to attempt substrate translocation. The errors of the measured ATPase rates were estimated to be +/- 10% based on three repeats.

Supplementary Figure 3

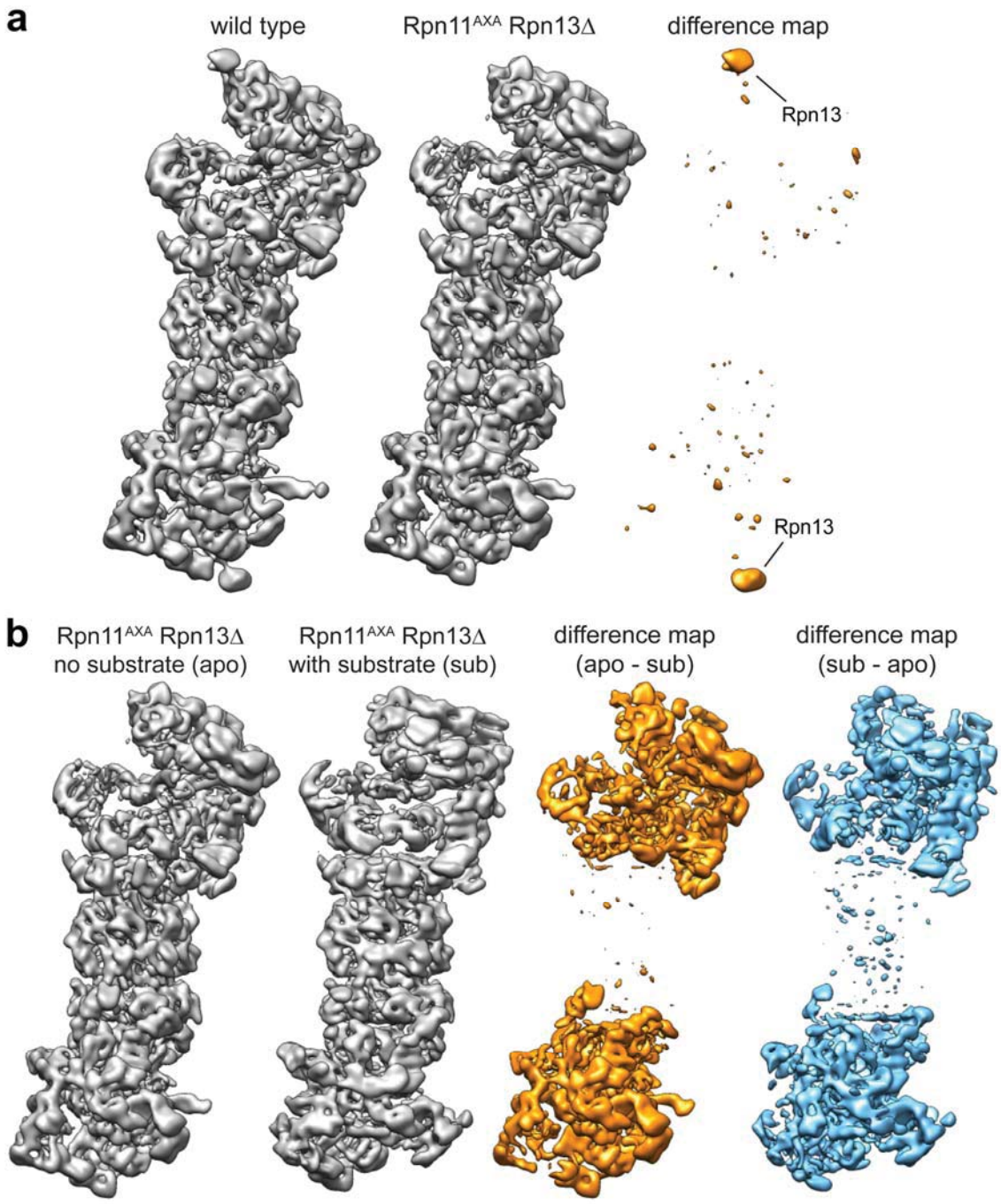

c

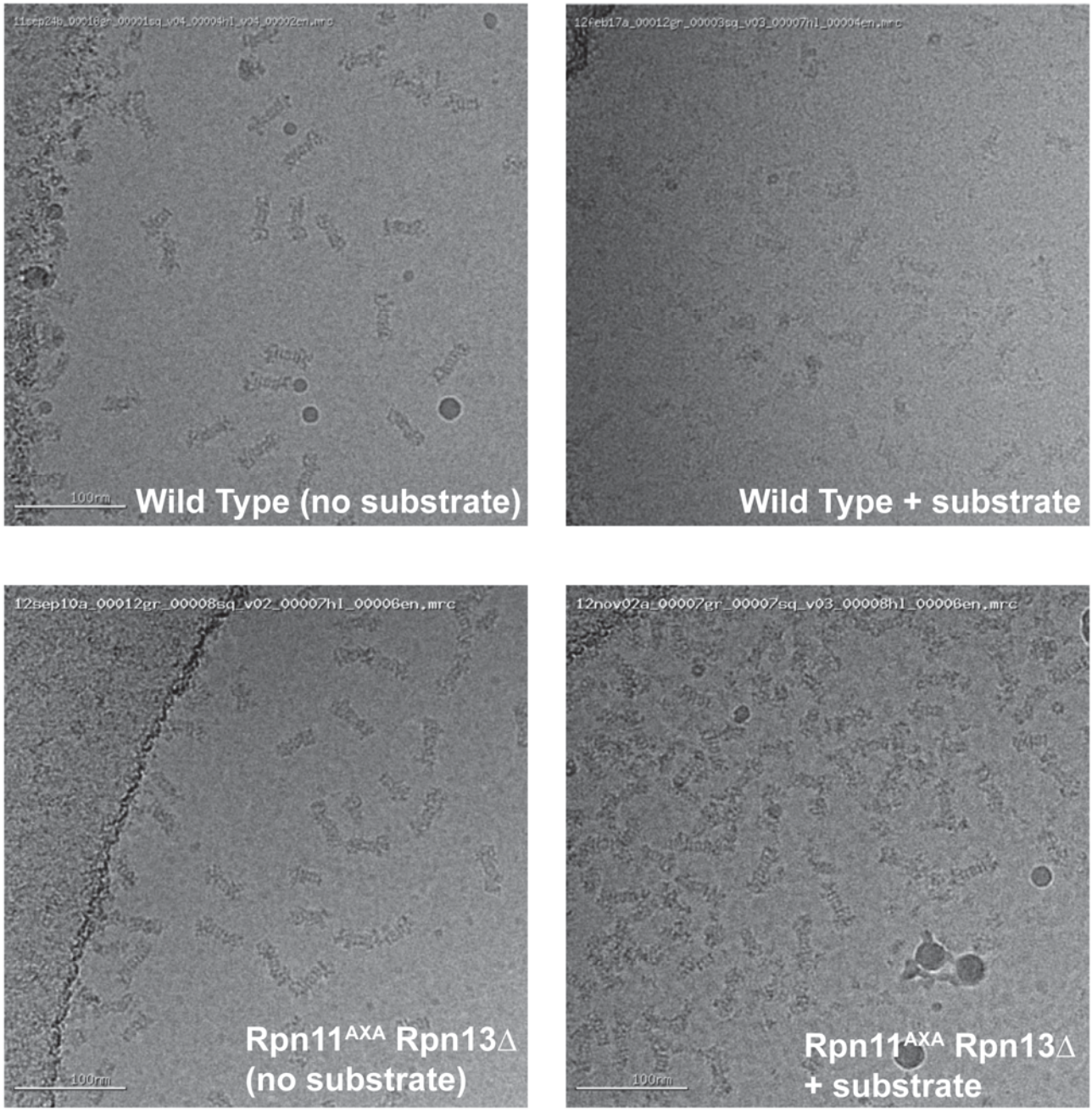

Supplementary Figure 3. Structural comparison of wild-type and Rpn11^{AXA} Rpn13Δ proteasomes and their resolution on micrographs in the absence and presence of substrate. (**a**) Rpn11^{AXA} ΔRpn13 reconstruction difference maps. The subnanometer-resolution cryo-EM reconstructions of the substrate-free wild-type (left) and Rpn11^{AXA} Rpn13Δ mutant (middle) proteasomes are shown as surface representations in the same orientation. A difference map of the mutant and wild-type reconstructions (right, gold) revealed no notable differences in the architecture of the two structures, which the exception of Rpn13, which is absent from the mutant. (**b**) Positive and negative difference maps (right, gold, and blue, respectively) of the mutant proteasome in the absence (apo) and presence (sub) of substrate (left, gray) indicate that there is a substantial rearrangement of the regulatory particle upon substrate binding. All difference maps were generated using the program diffmap.exe (N. Grigorieff Lab). **(c)** Micrographs of frozen-

hydrated proteasome particles. Wild type proteasomes in the absence of substrate (top left) are observed with high contrast, while the addition of excess substrate severely decreases the signal-to-noise ratio of holoenzyme particles (top right). Rpn11^{AXA} Rpn13Δ proteasomes in the absence of substrate (bottom left) are indistinguishable from wild-type particles, and the addition of substrate in two-fold excess does not negatively impact the signal-to-noise ratio. The micrographs displayed were all taken in areas of similar ice thickness, and imaged using a dose of 20e-/Å2 at a defocus of 2 (+/- 0.1) microns.

Supplementary Figure 4

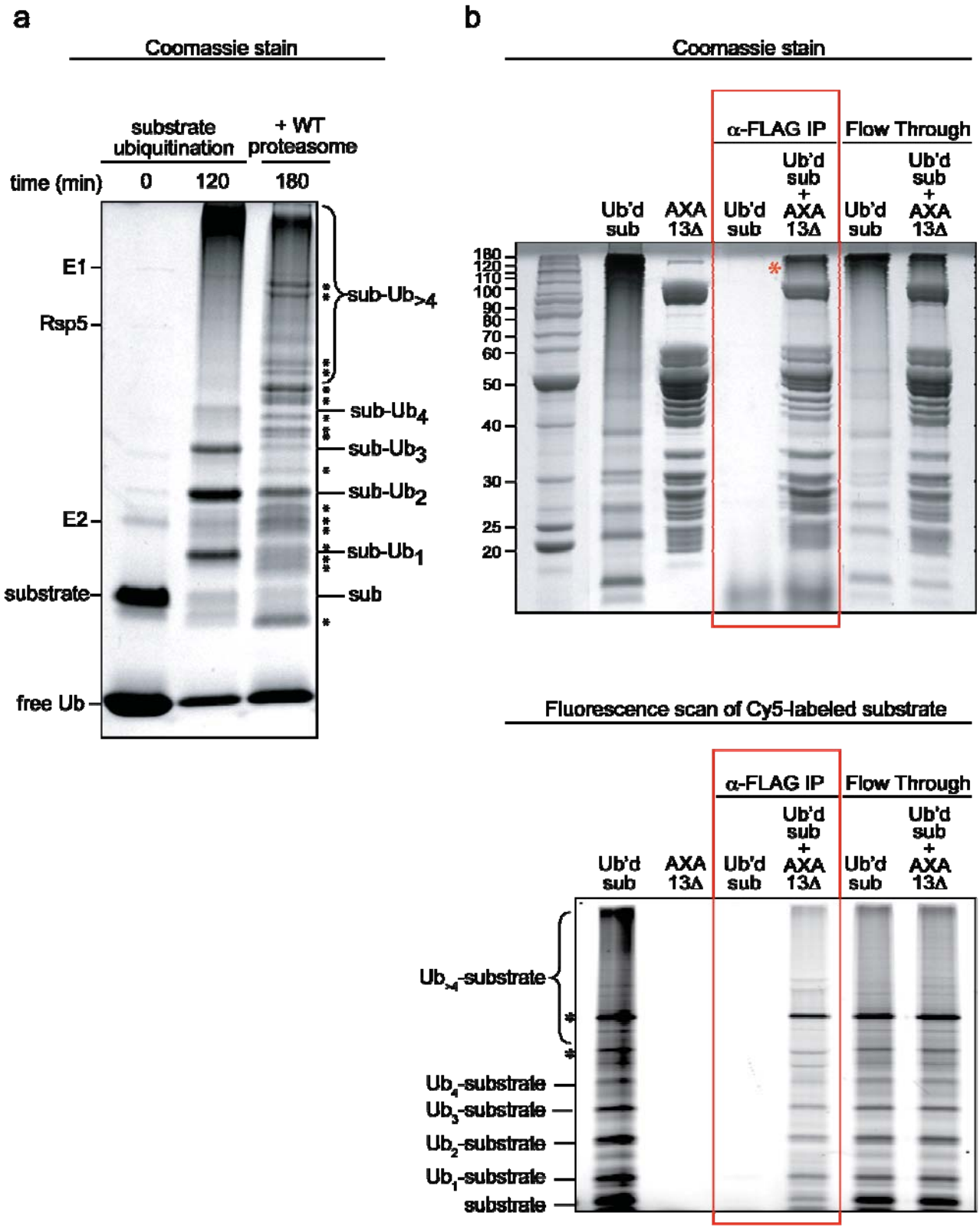

Supplementary Figure 4. G3P fusion substrate can be degraded by wild-type proteasome and stably binds to Rpn11^{AXA} Rpn13Δ proteasome. (**a**) Coomassie-stained gel (12%, NuPAGE) showing the ubiquitination of the G3P fusion substrate and its degradation by wild-type (WT) proteasome. A zero time point (left lane) shows all reaction components (labeled on left side) and a 120 min time point shows the complete ubiquitination of the substrate (middle lane, bands for

ubiquitinated substrate species labeled on right side). Wild-type holoenzyme and ATP regeneration mix were then added, and the degradation was analyzed after an additional 60 min (right lane, 180). Bands corresponding to proteasome subunits are marked with an asterisk (*, right side). After 60 minutes incubation with holoenzyme, the majority of ubiquitin-tagged substrate was degraded. (**b**) **Top**, Coomassie-stained gel (10%, NuPAGE) of ubiquitinated G3P substrate immunoprecipitated with $Rpn11^{AXA}$ Rpn13Δ proteasome. Ubiquitinated substrate (Ub'd sub) in the presence or absence of $Rpn11^{AXA}$-3XFLAG Rpn13Δ proteasomes (AXA 13Δ) was incubated with anti-FLAG M2 affinity resin and ATP regeneration mix for 5 min. The beads were then pelleted, the flow-through removed, and the beads washed 3 times. In the absence of proteasome, ubiquitinated substrate did not bind to the beads (α-FLAG IP, Ub'd sub) and was found entirely in the flow through (Flow Through, Ub'd sub). When proteasome was bound to the beads, an approximately stoichiometric amount of ubiquitinated substrate (red asterisk) was pulled down with the proteasome (α-FLAG IP, Ub'd sub + AXA 13Δ). Bands for substrate species with shorter ubiquitin chains (<5) were obscured by the bands for proteasome subunits. The flow through of this sample is shown on the right (Flow Through, Ub'd sub + AXA 13Δ). **Bottom**, To visualize pulled-down substrates with shorter ubiquitin chains and confirm the identity of the high-molecular weight material, we utilized a Cy5-labeled G3P substrate. This substrate was ubiquitinated and immunoprecipitated with $Rpn11^{AXA}$ Rpn13Δ proteasome under the same conditions as described above. Samples were separated on a SDS-PAGE gel (10%, NuPAGE), and visualized on a Typhoon Trio Imager (GE Healthcare). In the absence of proteasome, ubiquitinated substrate did not bind to the beads (α-FLAG IP, Ub'd sub). When proteasome was immobilized on the beads, the ubiquitinated Cy5-labeled substrate was pulled down (α-FLAG IP, Ub'd sub + AXA 13Δ).

Supplementary Figure 5

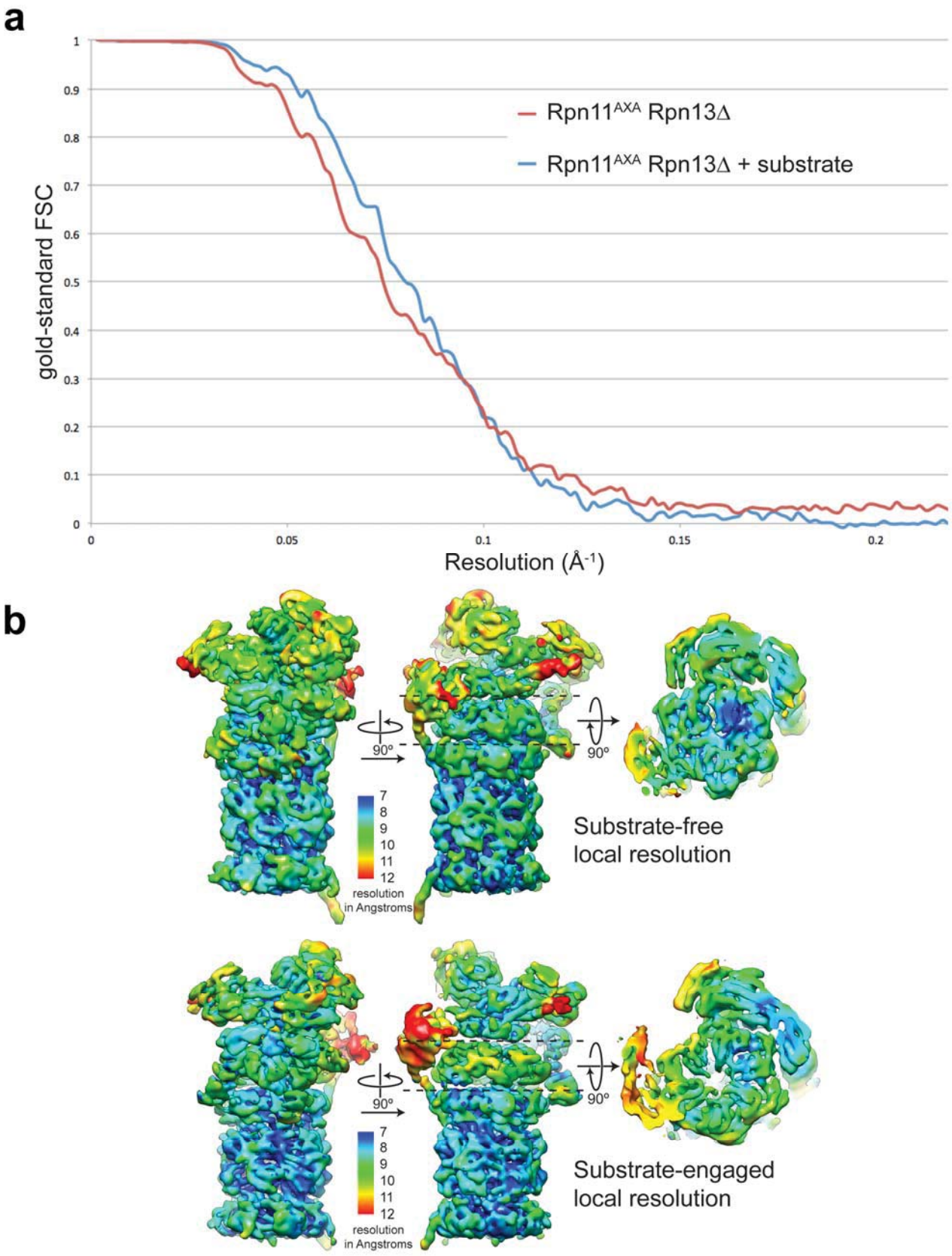

c

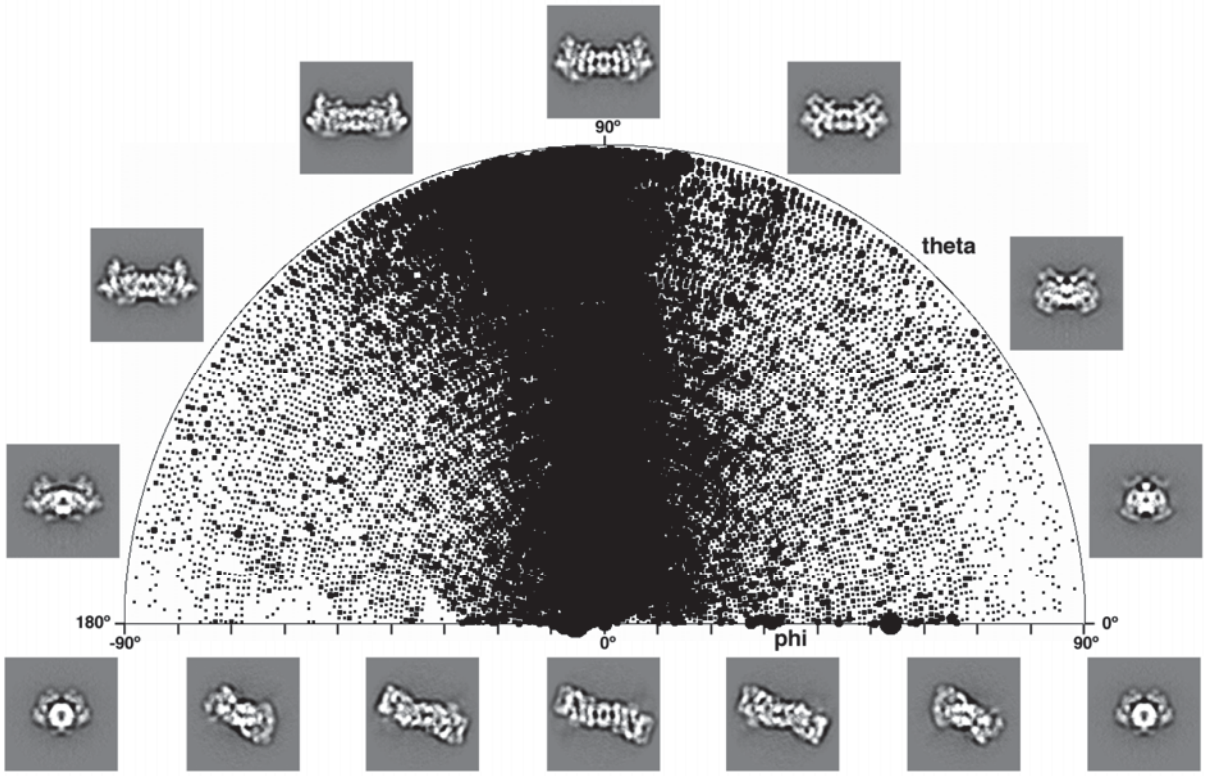

Angular distribution of substrate-free particles

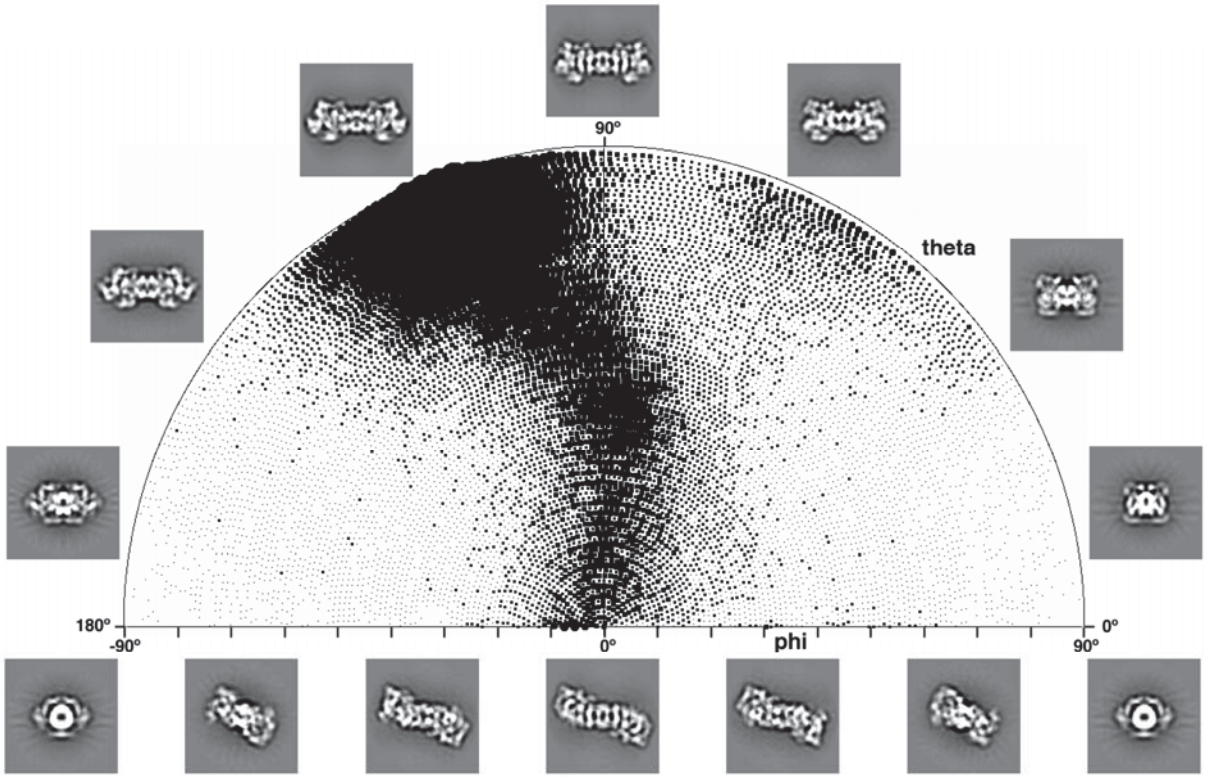

Angular distribution of substrate-engaged particles

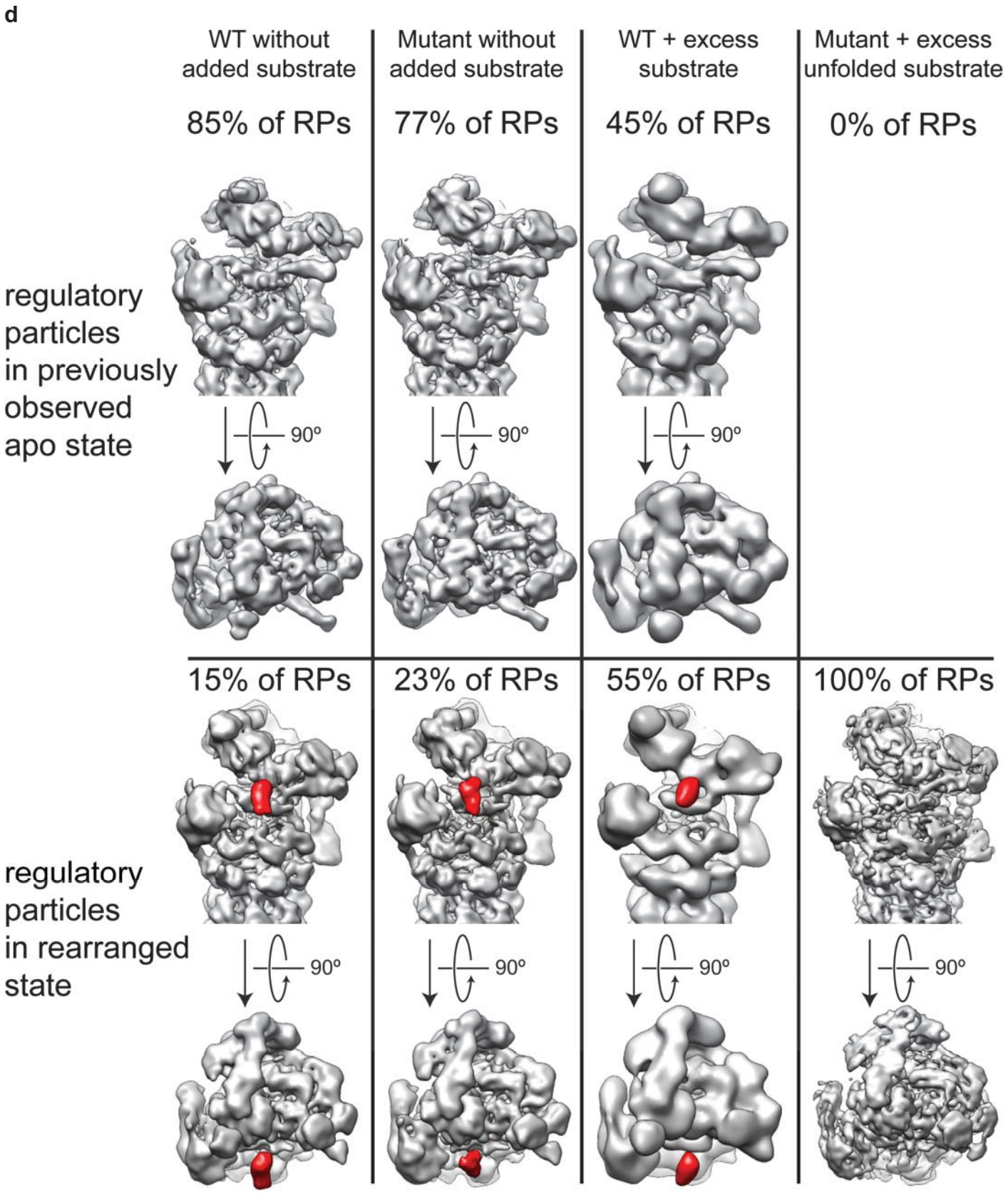
d
WT without added substrate
Mutant without added substrate
WT + excess substrate
Mutant + excess unfolded substrate
85% of RPs
77% of RPs
45% of RPs
0% of RPs
regulatory particles in previously observed apo state
90°
90°
90°
15% of RPs
23% of RPs
55% of RPs
100% of RPs
regulatory particles in rearranged state
90°
90°
90°
90°

e

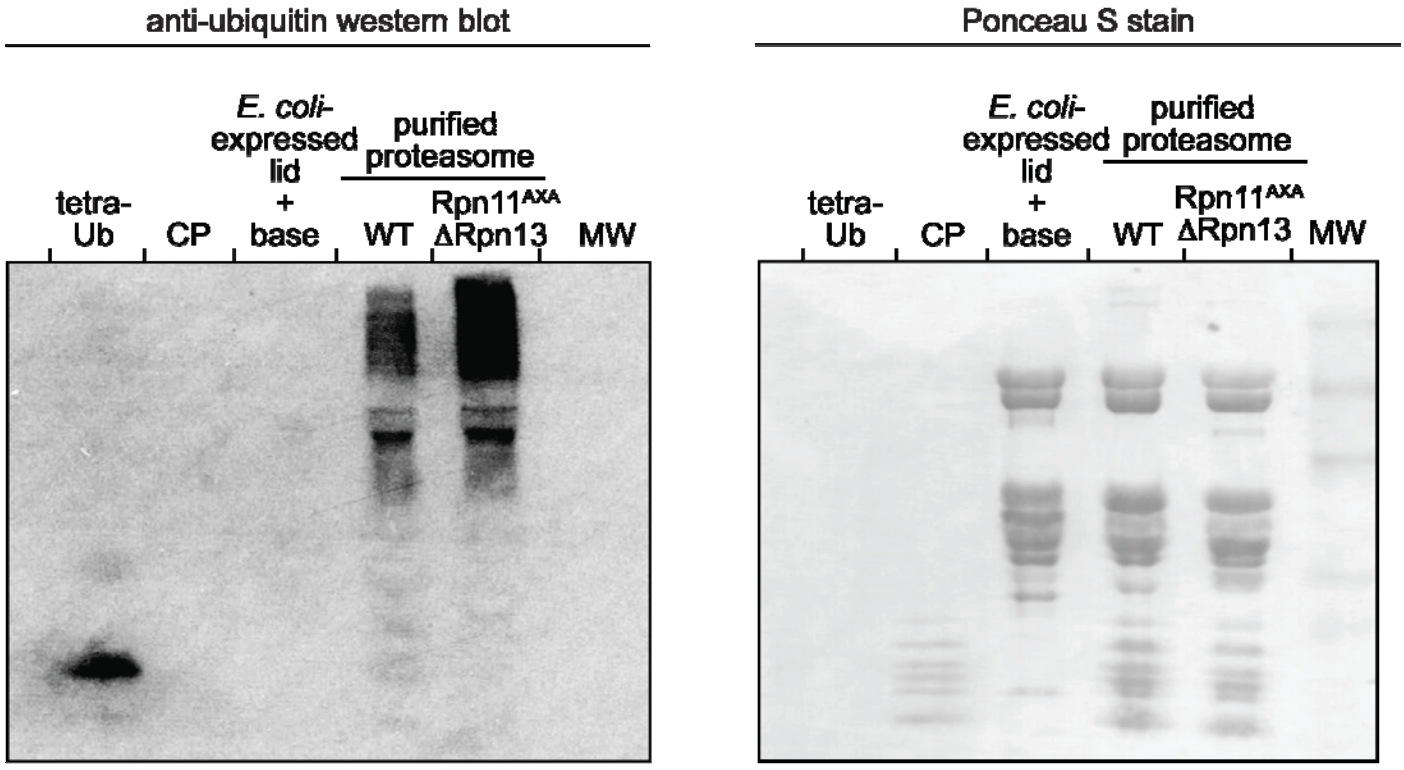

Supplementary Figure 5. Assessment of the resolution of Rpn11^{AXA} Rpn13Δ reconstructions and the percentage of "apo" proteasome particles engaged with endogenous substrate. (**a**) Gold-standard Fourier Shell Correlation (FSC) curves from independently processed half-datasets indicate that the Rpn11^{AXA} Rpn13Δ reconstructions in the absence (red line) and presence (blue line) of substrate are resolved to subnanometer resolution. (**b**) Local resolution calculations of the proteasome reconstructions are shown on the bottom right. The section of these local resolution maps that contains the AAA+ ring (the density between the dotted lines) is shown on the far right, displaying their relative difference in resolution. (**c**) The Euler distribution plots for the reconstructions of the AXA mutant in the absence (top) and presence (bottom) of substrate are shown. Forward-projections of the reconstructions are positioned around the axes, demonstrating the orientations of particles corresponding in that Euler space. Interestingly, the addition of substrate to the proteasome particles induced a preferred orientation of the holoenzyme in ice, explaining the necessity for a much larger substrate-bound dataset to achieve the same resolution as the substrate-free structure. (**d**) A percentage of "apo" particles are engaged with endogenous substrate and exhibit extra, substrate-related electron density. Wild-type (WT) and Rpn11^{AXA} Rpn13Δ mutant proteasome datasets were reprocessed using multi-model projection matching in order to probe for the presence of the rearranged conformation in the absence of added model substrate (left two columns, see materials and methods). A percentage of the regulatory particles (RPs) in these apo (no added substrate) datasets exhibited a conformational state associated with the substrate-engaged structure, but importantly, an additional density attributed to substrate (colored in red in the lower panels) accompanies this conformer. It is likely that these proteasomes were actively degrading endogenous substrate and in the process of unfolding a globular domain at the time of proteasome preparation and sample freezing for imaging. Keeping proteasome samples at low temperatures (≤ 4°C) throughout the purification may have stalled degradation and facilitated this co-purification of engaged or partially degraded endogenous substrates[1]. The presence of ubiquitin-tagged proteins

in these proteasome samples was confirmed by α-ubiquitin Western blotting (see below). After addition of GFP model substrate, 55% of wild-type regulatory particles show the substrate-engaged conformation and the extra small density attributed to the globular substrate portion (third column). For the deubiquitination-deficient AXA mutant, addition of the labile G3P substrate with a terminal ubiquitin tag causes all regulatory particles to switch to the substrate-engaged conformation (last column). Substrate density is not observable in this AXA-mutant reconstruction, since the substrate was designed such that the proteasome stalls after the globular G3P domain has been unfolded. (**e**) Endogenous ubiquitinated substrates co-purify with both wild-type and $Rpn11^{AXA}$ ΔRpn13 proteasome. **Left**, Anti-ubiquitin western blot analysis (using anti-serum for the P4D1 antibody, Santa Cruz Biotechnology, catalog # sc-8017, at 1:100) of equal amounts of purified wild-type (WT) and deubiquitination-deficient ($Rpn11^{AXA}$ ΔRpn13) proteasome shows the co-purification of ubiquitinated proteins from yeast. Importantly, 20S peptidase (CP) purified from yeast did not show any co-purification of ubiquitinated proteins. Furthermore, an equivalent amount of bacterially-expressed lid [3] and base (our unpublished data) exhibited no cross-reactivity with the antibody, confirming that the signal observed for the purified holoenzymes is indeed arising from co-purified ubiquitinated substrates. $Rpn11^{AXA}$ Rpn13Δ proteasome pulled down more ubiquitinated proteins than wild-type proteasome, a consequence of its deubiquitination deficiency. Tetra-ubiquitin (tetra-Ub) is shown as a positive control. **Right,** Ponceau S stain of the blot showing equal loading of purified proteasomes and subcomplexes. The far right lane contains molecular weight ladder (MW).

Supplementary Figure 6

a

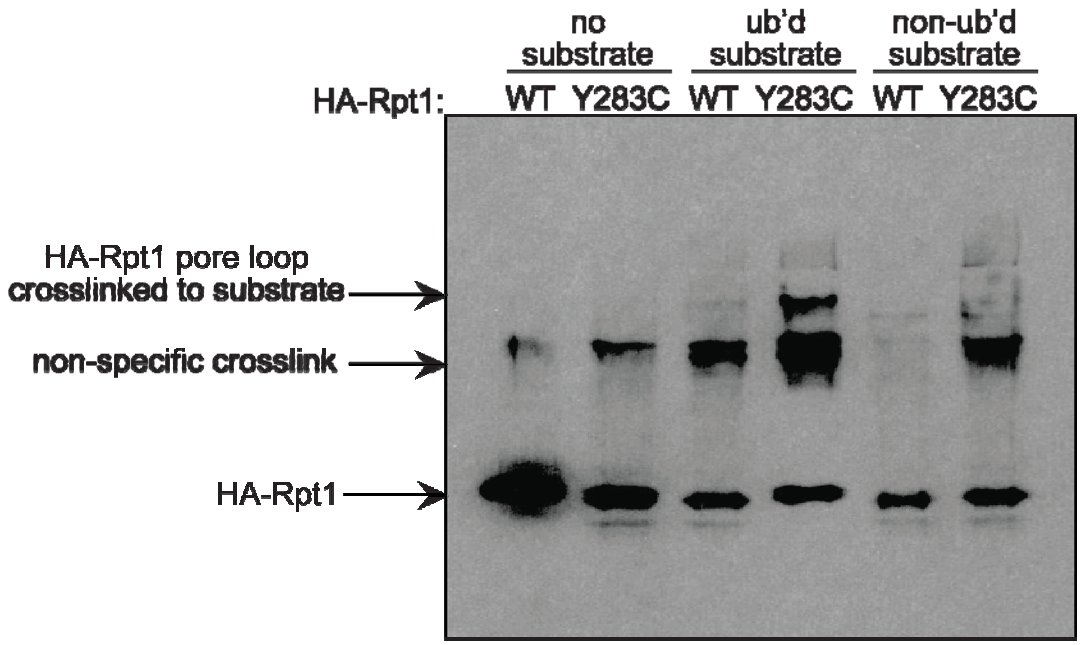

b

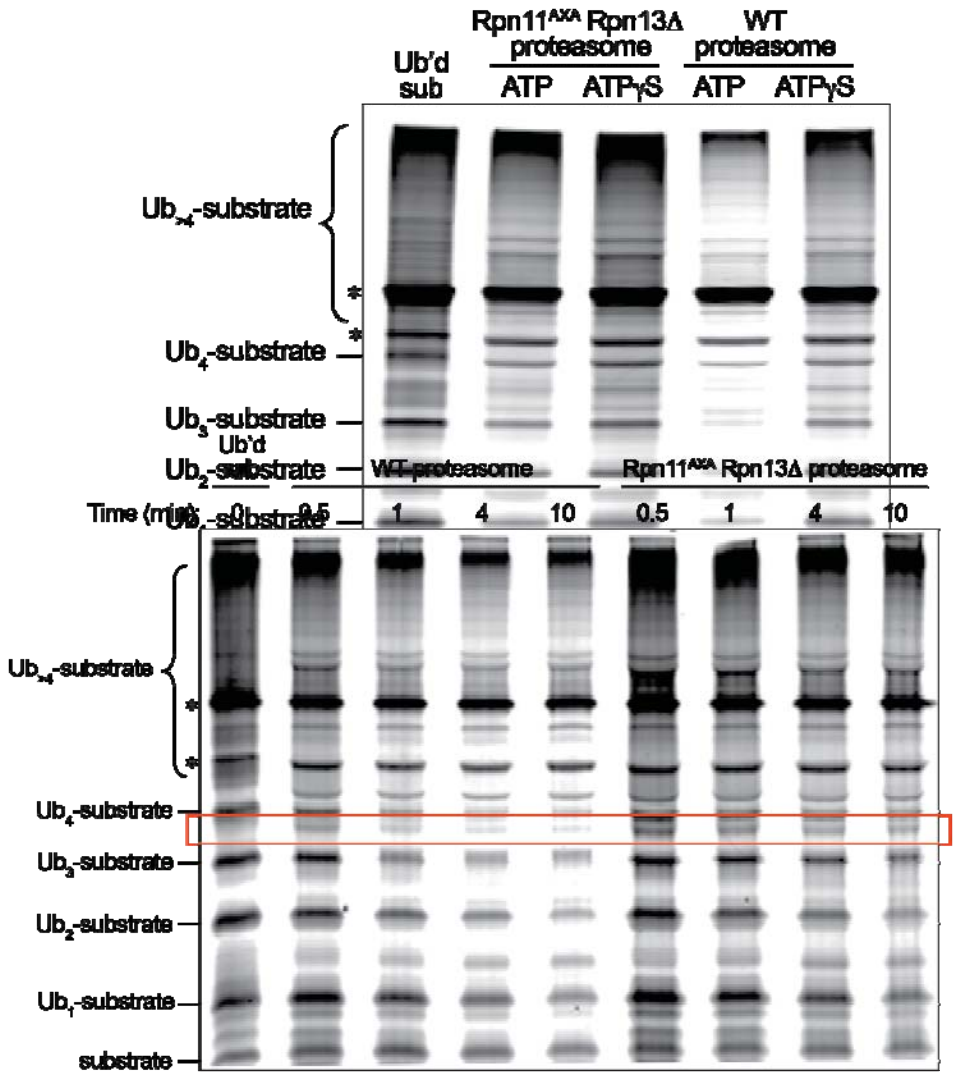

c

Supplementary Figure 6. Substrate is translocated through the central pore of Rpn11^{AXA} Rpn13Δ proteasome. (**a**) Disulfide crosslink between the pore-1 loop of Rpt1 and a translocating substrate. Anti-HA western blot showing specific crosslinks between the pore loop of HA-Rpt1 and ubiquitinated G3P substate. A G3P substrate containing a cysteine introduced 37 residues from the C-terminus (the start of proteasome degradation) was ubiquitinated and its cysteine residue activated for crosslinking by formation of a mixed disulfide with 5,5'-dithiobis-(2-nitrobenzoic acid) (DTNB). This substrate was incubated with a proteasome mutant containing Rpn11^{AXA} and either a wild-type (WT) Rpt1 or an Rpt1 bearing a cysteine mutation in its pore-1 loop (Rpt1 Y283C). Both Rpt1 variants contained an N-terminal HA-tag, allowing the specific detection of crosslinked species by α-HA western blotting after non-reducing SDS-PAGE. Since the G3P cysteine was placed in the middle of the polypeptide chain, crosslinking with the Rpt1 cysteine in the central pore is expected only upon successful translocation of the substrate. TNB-activated substrate that was not ubiquitinated and therefore not degraded served as a negative control to assess substrate-independent or non-specific crosslinking of Rpt1 to other Cys-containing proteasome subunits. Wild-type Rpt1 without a Cys in the pore loop showed some crosslinking to substrate, likely through other cysteines on the Rpt1 surface. Significant pore-specific crosslinks to Rpt1 were observed only in the presence of the ubiquitinated substrate, confirming that this substrate was successfully translocated through the central pore of the Rpn11^{AXA} mutant proteasome. (**b**) Substrate degradation by wild-type and deubiquitination-deficient proteasome. G3P substrate was labeled with Cy5-maleimide on an N-terminal cysteine and subsequently ubiquitinated (Ub'd sub, with non-substrate background bands indicated by asterisks). This ubiquitinated substrate (4 μM) was incubated with wild-type (WT) or Rpn11^{AXA} Rpn13Δ proteasome (2 μM) for 30 min in the presence of either ATP regeneration mix or ATPγS. Samples were then separated by SDS-PAGE and scanned for fluorescence using a Typhoon Trio Variable Mode Imager (GE Healthcare). After 30 min, wild-type proteasome in the presence of ATP had degraded the majority of substrate, while the Rpn11^{AXA} Rpn13Δ proteasome had processed only a fraction. That the degradation observed is indeed translocation-dependent was confirmed through the significant inhibition by ATPγS, which slows translocation by the AAA+ unfoldase. **(c)** Early time points for the degradation of Cy5-labeled G3P substrate by wild-type or Rpn11^{AXA} Rpn13Δ proteasome reveal partially degraded intermediates. Ubiquitinated substrate (Ub'd sub) was mixed rapidly with an equal amount of proteasome (2 μM substrate, 2 μM proteasome), and aliquots were removed at different time points for separation by SDS-PAGE and fluorescence scanning. Degradation intermediates (red box) can be observed after incubation with either wild-type or Rpn11^{AXA} Rpn13Δ proteasome,

indicating that deubiquitination may be a slow step in substrate processing even for the wild-type enzyme. However, for the deubiquitination-deficient Rpn11^{AXA} Rpn13Δ proteasome these intermediates are more abundant and longer persisting, as expected given the requirement for co-degradation rather than removal of the ubiquitin chain. It is still unknown whether an uncleaved ubiquitin chain slows down degradation because the thermodynamically stable ubiquitin is difficult to unfold or because processing of an ubiquitin chain requires the simultaneous translocation of several polypeptides through the proteasome pore. In either model, there is not a specific point at which the translocation stalls, which may explain the lack of numerous distinct bands for truncated substrate species.

Supplementary Figure 7

a

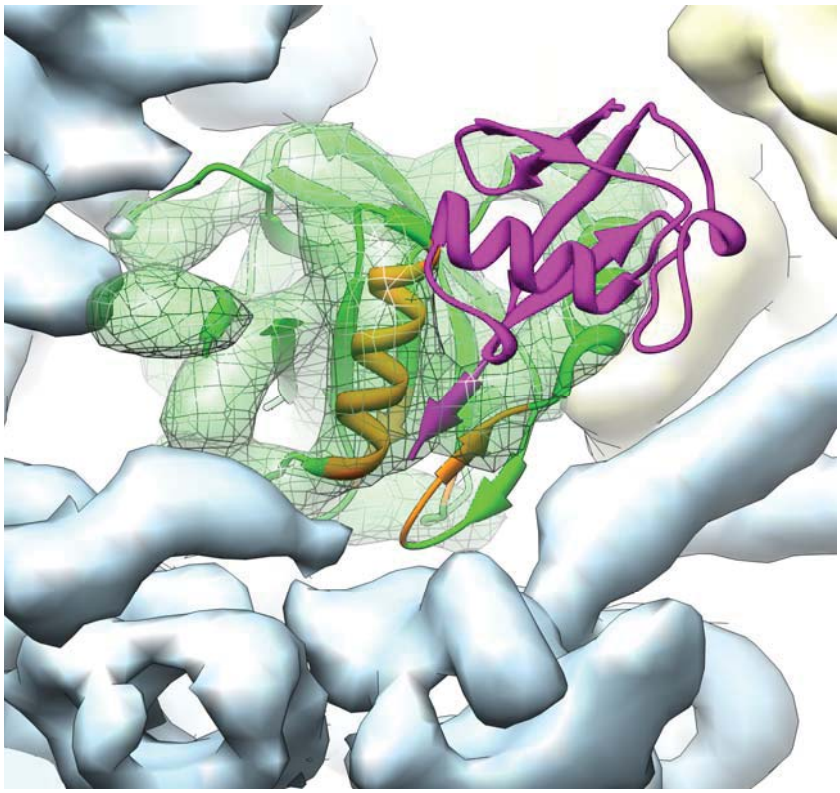

b

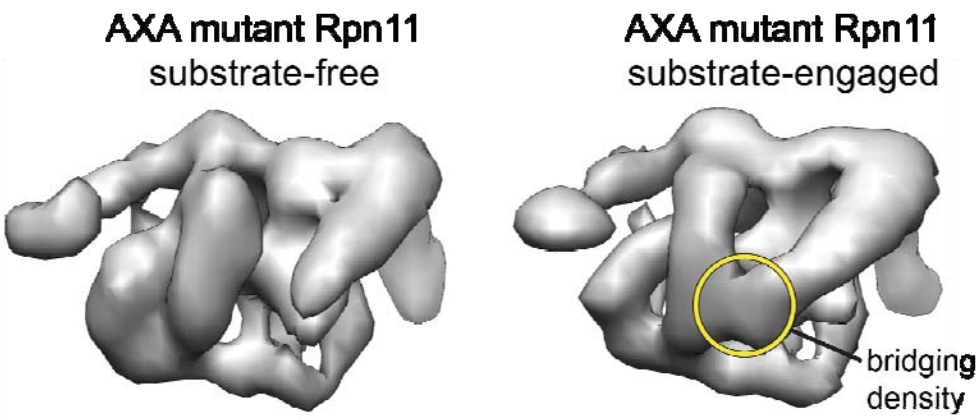

C

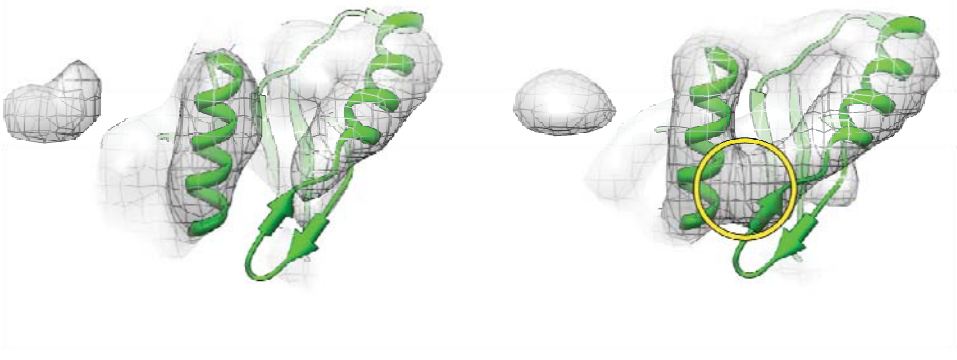

Supplementary Figure 7. Modeling and analysis of Rpn11 density in Rpn11^{AXA} Rpn13Δ reconstructions. (**a**) Proposed interaction between Rpn11 and ubiquitin. Using the crystal structure of the ubiquitin-bound DUB AMSH-LP as a structural reference [4], an ubiquitin moiety (magenta) was modeled into the Rpn11 catalytic groove (orange residues within green ribbon). The bridging density across the catalytic groove likely corresponds to the bound C-terminal tail of ubiquitin, which adds a third strand to an existing two-stranded beta sheet, as observed in AMSH-LP [4]. (**b**) Comparison of Rpn11 density in AXA reconstructions. The segmented densities corresponding to Rpn11 in the Rpn11^{AXA} Rpn13Δ proteasome in the absence (left) and presence (right) of substrate are shown. At subnanometer resolution the secondary structural elements are discernible, and shows that the subunit does not undergo a conformational reorganization upon substrate engagement. Of note is a bridging density that appears at the catalytic groove. (**c**) The surface representation from (a) is shown, emphasizing the two helices of the catalytic groove docked in position. The bridging density observed between these helices is located at Rpn11's putative site of interaction with an ubiquitin tail.

Supplementary Figure 8

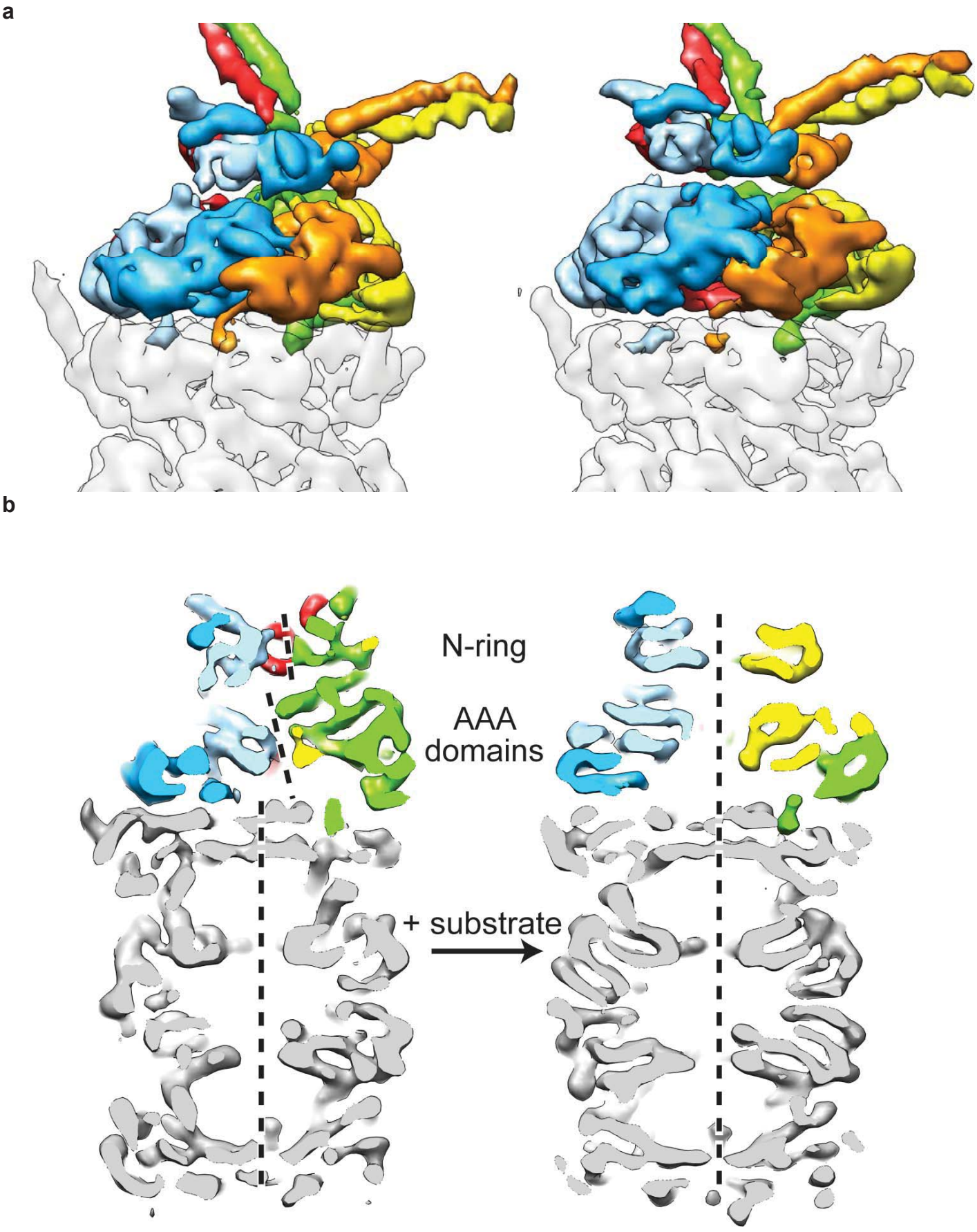

Supplementary Figure 8. Substrate-induced rearrangements of the ATPase subunits allow coaxial alignment of the base and 20S peptidase, but do not affect docking of the C-terminal tails of Rpt2, Rpt3, and Rpt5 with the peptidase. (**a**) The C-terminal tails of Rpt2, Rpt3, and Rpt5 dock into the alpha pockets of the 20S peptidase in both the substrate-free and substrate-engaged structures. The segmented electron densities corresponding to the ATPase subunits Rpt1-Rpt6 (rainbow) and the peptidase (transparent) are shown for the $Rpn11^{AXA}$ Rpn13Δ proteasome in the absence (left) and presence (right) of substrate. Density for the C-terminal tails of Rpt2 (light blue), Rpt3 (green), and Rpt5 (orange), which contain the conserved HbYX motif, can be observed docked into their cognate 20S peptidase binding pockets at the interfaces of the subunits α3 and α4, α1 and α2, and α5 and α6, respectively, in both the substrate-free and substrate-bound conformation. Density was not observed for the tails of Rpt1 (dark blue), Rpt4 (yellow), and Rpt6 (red) in either state. (**b**) Coaxial alignment of the ATPase subunits and the peptidase. Cross-sections of the substrate-free (left) and substrate-engaged (right) reconstructions are shown, with the ATPase multicolored and the peptidase in grey. Dotted lines indicate the paths of the central channels through the N-ring, AAA-ring, and peptidase, demonstrating the significant deviations from a coaxial alignment in the substrate-free state.

Supplementary Table 1. Strain List

Strain	Genotype	Source
YYS40	*MAT***a** *ade2-1 his3-11,15 leu2-3,112 trp1-1 ura3-1 can1-100 RPN11::RPN11-3XFLAG (HIS3)*	Y. Saeki
DOM90 (AFS92)	*MAT***a** *ade2-1 his3-11,15 leu2-3,112 trp1-1 ura3-1 can1-100 bar1*	A. Straight
yAM11	*MAT***a** *ade2-1 his3-11,15 leu2-3,112 ura3-1 can1-100 trp1-1::P_{RPN11}-rpn11AXA-3XFLAG-TRP1(pRS304) rpn13Δ::KanMX*	This study
yAM12	*MAT***a** *ade2-1 his3-11,15 ura3-1 can1-100 trp1-1::P_{RPN11}-rpn11AXA-3XFLAG-TRP1(pRS304) rpn13Δ::KanMX leu2-3,112::P_{RPT1}-HA-RPT1-LEU2(pRS305)*	This study
yAM13	*MAT***a** *ade2-1 his3-11,15 ura3-1 can1-100 trp1-1::P_{RPN11}-rpn11AXA-3XFLAG-TRP1(pRS304) rpn13Δ::KanMX leu2-3,112::P_{RPT1}-HA-rpt1Y283C-LEU2(pRS305)*	This study

Supplementary Movie 1. Structural rearrangements in the proteasome regulatory particle that occur upon substrate engagement. Substrate-induced conformational changes include a rearranged ATPase ring with uniform subunit interfaces, a widened central channel coaxially aligned with the peptidase, and a spiral orientation of pore loops that suggests a rapid progression of ATP-hydrolysis events around the ring. Importantly, Rpn11 moves from an occluded position to directly above the central pore, facilitating substrate deubiquitination concomitant with translocation.

References

1 Peth, A., Uchiki, T. & Goldberg, A. L. ATP-dependent steps in the binding of ubiquitin conjugates to the 26S proteasome that commit to degradation. *Mol Cell* **40**, 671-681, doi:S1097-2765(10)00840-3 [pii]10.1016/j.molcel.2010.11.002 (2010).

2 Kenniston, J. A., Baker, T. A., Fernandez, J. M. & Sauer, R. T. Linkage between ATP consumption and mechanical unfolding during the protein processing reactions of an AAA+ degradation machine. *Cell* **114**, 511-520, doi:S0092867403006123 [pii] (2003).

3 Lander, G. C. *et al.* Complete subunit architecture of the proteasome regulatory particle. *Nature* **482**, 186-191, doi:nature10774 [pii]10.1038/nature10774 (2012).

4 Sato, Y. *et al.* Structural basis for specific cleavage of Lys 63-linked polyubiquitin chains. *Nature* **455**, 358-362, doi:nature07254 [pii]10.1038/nature07254 (2008).

5 Pathare, G. R. *et al.* The proteasomal subunit Rpn6 is a molecular clamp holding the core and regulatory subcomplexes together. *Proc Natl Acad Sci U S A* **109**, 149-154, doi:1117648108 [pii]10.1073/pnas.1117648108 (2011).

6 Beck, F. *et al.* Near-atomic resolution structural model of the yeast 26S proteasome. *Proc Natl Acad Sci U S A* **109**, 14870-14875, doi:10.1073/pnas.1213333109 (2012).